

Features of ω photoproduction off nucleon target at forward angles : Dominance of π exchange with Regge cuts and scaling of differential cross sections

Byung-Geel Yu*

Research Institute of Basic Science, Korea Aerospace University, Goyang, 10540, Korea

Tae Keun Choi†

Dept. of Physics, Yonsei University, Wonju, 220-710, Korea

Kook-Jin Kong‡

Research Institute of Basic Science, Korea Aerospace University, Goyang, 10540, Korea

We investigate photoproduction of ω off a nucleon target $\gamma N \rightarrow \omega N$ by using a Reggeized model where $\pi(135) + \sigma(500) + f_1(1285) + f_2(1270) + \text{Pomeron}$ exchanges are included in the t -channel for the reaction at forward angles. The reaction mechanism at low energy is featured by the dominance of the π exchange with the absorptive cuts introduced to modulate the pion contribution to both $\gamma p \rightarrow \omega p$ and $\gamma n \rightarrow \omega n$ reactions. Necessity of σ exchange is illustrated in the analysis of the cross section from natural parity exchanges. Cross sections for differential, total, and spin density matrix with parity and beam polarization asymmetries are reproduced and compared with existing data on $\gamma p \rightarrow \omega p$. Scaled differential cross sections of Jefferson Lab data on $\gamma p \rightarrow \omega p$ are investigated at the production angle $\theta = 90^\circ$ with the nonlinear trajectories for a saturation. Differential and total cross sections for the $\gamma n \rightarrow \omega n$ reaction are analyzed to compare with recent experimental data at the CBELSA/TAPS Collaboration. An application to the $\gamma p \rightarrow \omega \Delta^+$ reaction is presented to demonstrate the significance of the π exchange in the total and differential cross sections.

PACS numbers: 11.55.Jy, 13.40.-f, 13.60.Le

I. INTRODUCTION

Photoproductions of lighter vector mesons, ρ^0 , ω , and ϕ are important to study hadron reactions because they provide information to understand the diffractive scattering that leads to a discovery of the Pomeron [1]. Among these reactions photoproduction of ω , in particular, shows a feature quite distinctive from others in the low energy region by the special role of the π exchange. Given the decay width $\omega \rightarrow \pi^0 \gamma$ especially large, the role of π exchange appears to be prominent more than the cases in the ρ^0 and ϕ processes near threshold [2]. Furthermore, as an application to nuclear reactions to observe vector meson properties in nuclear medium [3], the recent 12 GeV upgrade of the Jefferson Lab facilities with the GlueX detector draws attention because the knowledge about ω photoproduction becomes even more important to understand QCD dynamics through the color transparency in the nuclear photoproduction of ω [3, 4]. Therefore, all these topics need for a comprehensive study of ω photoproduction on the nucleon target through the systematic approach to the analysis of the empirical data [5].

In this work we elaborate to construct a model for ω photoproduction at forward angles and attempt to describe the production mechanism throughout the reaction energy from threshold to hundreds of GeV region

where only the Pomeron exchange is prevailing. For this purpose, we utilize the Regge model of Ref. [6] where the t -channel meson exchanges $\pi + \sigma + f_2$ are included without either fit parameters for coupling strength or form factors to cutoff divergences. Within the Reggeized framework the roles of lighter mesons π and σ are worth investigating, because the former exchange with the large couplings of $\gamma \pi \omega$ and $\pi N N$ gives the contribution too excessive to agree with the observed cross section and the latter exchange plays the role more important than the π exchange in the peaking of ρ^0 [2, 7] and ϕ cross sections near threshold [6].

To clarify the roles of these nonresonant meson exchanges the measurement of the $\gamma p \rightarrow \omega p$ process at the SLAC/LBL Collaborations in Ref. [8] is useful because the reaction cross section is provided in a separate manner into the natural and the unnatural parity exchanges respectively at photon energies 2.8, 4.7, and 9.3 GeV. This enables us to investigate meson exchanges of different parities independently, because they do not interfere with each other. More recently, experiments on ω photoproduction are extended to include the reaction at the deuteron target and the data on the reaction off a neutron target from the CBELSA/TAPS and GRAAL Collaborations [9, 10] are available for photon energies up to 2 GeV. From the isospin symmetry, therefore, photoproduction of ω off the neutron target could provide further constraint on the different role of the π exchange in the isovector channel.

The scaling of the differential cross section is one of the interesting phenomena observed in hadron reactions at wide angles, or alternatively large $-t$. According to

* bgyu@kau.ac.kr

† tkchoi@yonsei.ac.kr

‡ kong@kau.ac.kr

the dimensional scaling predicted from pQCD calculation [11], the reaction around mid angle, i.e., the production angle $\theta \approx 90^\circ$, shows a scaling of cross section as the reaction energy increases [6, 12, 13]. Thus, quark evidences in photoproduction of hadrons could be searched for and the measurement of cross section for $\gamma p \rightarrow \omega p$ at the angle around $\theta = 90^\circ$ is also expected to offer an observation of the transition between hadronic and parton phases in the target nucleon. In the present framework which is specialized to describe the reaction at forward angles we make an analysis of the scaled differential cross sections by virtue of the saturation of the Regge trajectory valid at large $-t$.

In relation with the above issues it is worth investigating the reaction $\gamma p \rightarrow \omega \Delta^+$ in parallel with the ω photoproduction on nucleon, because the reaction has not been well understood yet with few experiments [14, 15] and theories [16]. Together with the $\gamma p \rightarrow \omega p$ reaction the knowledge of the reaction mechanism may help to analyze nuclear reactions including the study of color transparency in nuclear photoproduction of ω .

All the topics discussed above are our primary interest in the present work and this paper is organized as follows. In Sec. II we construct a model for the meson exchange which is reggeized in the t -channel. Contributions of the natural and unnatural parity exchanges are investigated, respectively, based on the SLAC/LBL data as discussed above. The role of σ in addition to f_2 +Pomeron exchanges is discussed in the natural parity cross section, while the necessity of the Regge cuts to modulate the π exchange is demonstrated for the $\gamma N \rightarrow \omega N$, which, otherwise, overestimates the unnatural parity cross section. Numerical consequence in $\gamma p \rightarrow \omega p$ reaction are presented in Sec. III for differential, total, and scaled differential cross sections. Spin polarizations including

spin density matrix and beam polarization are analyzed to compare with data over resonance region. Differential and total cross sections for $\gamma n \rightarrow \omega n$ process are calculated and given to compare with recent CBELSA/TAPS data. As an extension of the current framework, the application to $\gamma p \rightarrow \omega \Delta^+$ process is also presented to investigate the relevance of the π exchange with the cut. Section IV contains a summary and discussion.

II. THE REGGE MODEL

In this section we construct a photoproduction amplitude for the reaction

$$\gamma(k) + N(p) \rightarrow \omega(q) + N(p'), \quad (1)$$

which is able to describe the Pomeron exchange at high energies, while in the low and intermediate energy regions the nonresonant meson exchanges are to reproduce threshold peaking in the cross sections measured in experiments. Here k, p are the four-momenta of photon and nucleon in the initial state, and q, p' are the ω and the final nucleon momenta, respectively.

A. t -channel meson Regge poles at forward angles

Since the ω -meson itself is not allowed to exchange by charge conjugation, the meson exchanges relevant to the reaction in Eq. (1) are written as

$$\mathcal{M} = \mathcal{M}_\sigma + \mathcal{M}_{f_2} + \mathcal{M}_\mathbb{P} + \mathcal{M}_\pi + \mathcal{M}_{f_1}, \quad (2)$$

where the scalar meson, tensor meson, and Pomeron exchanges are

$$\mathcal{M}_\sigma = \frac{g_{\gamma\sigma\omega}}{m_0} g_{\sigma NN} (k \cdot q \eta^* \cdot \epsilon - \epsilon \cdot q \eta^* \cdot k) \bar{u}(p') u(p) \mathcal{R}^\sigma(s, t), \quad (3)$$

$$\mathcal{M}_{f_2} = \Gamma_{\gamma f_2 \omega}^{\beta\rho}(k, q) \Pi_{\beta\rho; \lambda\sigma}(Q) \bar{u}(p') \Gamma_{f_2 NN}^{\lambda\sigma}(p', p) u(p) \mathcal{R}^{f_2}(s, t), \quad (4)$$

$$\mathcal{M}_\mathbb{P} = 12i \frac{e \beta_q \beta_{q'}}{f_\omega} \frac{m_\omega^2}{m_\omega^2 - t} \left(\frac{2\mu_0^2}{2\mu_0^2 + m_\omega^2 - t} \right) e^{-i\frac{\pi}{2}[\alpha_\mathbb{P}(t)-1]} \left(\frac{s}{4s_0} \right)^{\alpha_\mathbb{P}(t)-1} F_1(t) \bar{u}(p') (\not{k} \eta^* \cdot \epsilon - \not{q} \eta^* \cdot k) u(p) \quad (5)$$

for the natural parity ($P = (-1)^J$), and the π and f_1 axial vector meson are

$$\mathcal{M}_\pi = i \frac{g_{\gamma\pi\omega}}{m_0} g_{\pi NN} \epsilon^{\mu\nu\alpha\beta} \epsilon_\mu \eta_\nu^* k_\alpha q_\beta \bar{u}(p') \gamma_5 u(p) \mathcal{R}^\pi(s, t), \quad (6)$$

$$\mathcal{M}_{f_1} = i \frac{g_{\gamma f_1 \omega}}{m_0^2} g_{f_1 NN} m_\omega^2 \epsilon_{\mu\nu\alpha\beta} k^\mu \eta^{\nu*} \epsilon^\alpha (-g^{\beta\lambda} + Q^\beta Q^\lambda / m_{f_1}^2) \left(\frac{1}{1 - t/M_A^2} \right)^2 \bar{u}(p') \gamma_\lambda \gamma_5 u(p) \mathcal{R}^{f_1}(s, t), \quad (7)$$

for unnatural parity ($P = -(-1)^J$) exchanges.

The Regge propagator is given by

$$\mathcal{R}^\varphi(s, t) = \frac{\pi \alpha_J' \times \text{phase}}{\Gamma[\alpha_J(t) + 1 - J] \sin[\pi \alpha_J(t)]} \left(\frac{s}{s_0} \right)^{\alpha_J(t) - J} \quad (8)$$

written in the collective form for the φ meson of spin- J which stands for all the mesons considered here. $s_0 = 1$ GeV². The phase factor is, in general, taken to be of the canonical form, $\frac{1}{2}[(-1)^J + e^{-i\pi\alpha_J(t)}]$, for each meson exchange. Photon and vector meson polarizations

are denoted by $\epsilon(k)$ and $\eta^*(q)$ with momenta k and q , respectively. $u(p)$ and $u(p')$ are the spinors for the initial and final nucleon with the momenta p and p' , respectively. $Q^\mu = (q - k)^\mu$ is the t -channel momentum-transfer and the dimensionful parameter $m_0 = 1$ GeV.

Natural parity exchange

- $\sigma(500) J^{PC} = 0^{++}$

Though the isoscalar σ meson plays an important role in reproducing the threshold peak of the ρ^0 and ϕ reactions [2, 6], it was excluded in previous studies [17, 18] by the uncertainty in the decay width. However, the Particle data group (PDG) reports that the partial widths $\Gamma_{\omega \rightarrow \pi^+ \pi^- \gamma} \approx 3.6 \times 10^{-3}$ and $\Gamma_{\omega \rightarrow \pi^0 \pi^0 \gamma} \approx 6.7 \times 10^{-5}$ which are comparable to those of ρ^0 and ϕ in magnitude. In practice the two pions can be associated with an s -wave propagation of σ as an effective degree of freedom. Thus, taking $\Gamma_{\omega \rightarrow \sigma \gamma} \approx \Gamma_{\omega \rightarrow \pi^+ \pi^- \gamma} \approx 30.56$ keV as the upper limit, we estimate $|g_{\gamma \sigma \omega}| \approx 0.53$, which is not negligible but rather larger than the radiative decays of other mesons. Moreover, such an estimate is consistent with the predictions either $\Gamma_{\omega \rightarrow \sigma \gamma} = 16 \pm 3$, or 33 ± 4 keV from the chiral effective Lagrangians incorporated with the vector meson dominance [19]. This yields $|g_{\gamma \sigma \omega}| \approx 0.22$ or 0.32 , respectively. In the present calculation, we take the smaller value $g_{\gamma \sigma \omega} = -0.17$ with the negative sign for the reason for a better agreement with the natural-parity cross section as shown in Fig. 1 (a). For the σNN coupling constant, we take $g_{\sigma NN} = 14.6$ [20] close to πNN coupling constant to be consistent with the chiral partner to the π in the σ model.

- $f_2(1270) J^{PC} = 2^{++}$

Following the isoscalar σ meson, the exchange of spin-2 tensor meson f_2 gives the contribution substantial to reproduce the reaction cross section in intermediate energies up to $\sqrt{s} \approx 10$ GeV. The coupling constants of f_2 exchange are obtained as $g_{\gamma f_2 \omega}/m_0 = 0.0376/m_0$ from the partial decay width $\Gamma_{f_2 \rightarrow \omega \gamma} = 27$ keV by the relativistic quark model prediction [21] and $g_{f_2 NN}^{(1)} = 6.45$ and $g_{f_2 NN}^{(2)} = 0$ for the tensor meson-nucleon couplings from Ref. [22]. Details of the coupling vertices $\Gamma_{\gamma f_2 \omega}^{\beta \rho}(k, q)$ and $\Gamma_{f_2 NN}^{\lambda \sigma}(p', p)$ are given in Ref [6]. The spin-2 projection is given by

$$\Pi_{(2)}^{\beta \rho; \sigma \lambda}(Q) = \frac{1}{2}(\bar{g}^{\beta \sigma} \bar{g}^{\rho \lambda} + \bar{g}^{\beta \lambda} \bar{g}^{\rho \sigma}) - \frac{1}{3} \bar{g}^{\beta \rho} \bar{g}^{\sigma \lambda}, \quad (9)$$

with $\bar{g}^{\mu \nu}(Q) = -g^{\mu \nu} + Q^\mu Q^\nu / m_{a_2}^2$.

- Pomeron $J^{PC} = 1^{-+}$

The concept and practical use of the exchange of vacuum quantum-numbers, so called the soft Pomeron, is to date well-established in photoproductions of lighter vector mesons. The Pomeron exchange of an isoscalar

TABLE I. Listed are the physical constants and Regge trajectories with the corresponding phase factors for $\gamma N \rightarrow \omega N$. φ stands for σ , π and f_2 . $f_2 NN$ coupling constants are understood as $g_{f_2 NN}^{(1)} = 6.45$ and $g_{f_2 NN}^{(2)} = 0$.

meson	trajectory(α_φ)	phase factor	$g_{\gamma \varphi \omega}$	$g_{\varphi NN}$
π for γp	$0.7(t - m_\pi^2)$	$e^{-i\pi\alpha_\pi}$	-0.69	13.4
π for γn	$0.7(t - m_\pi^2)$	1	-0.69	-13.4
σ	$0.7(t - m_\sigma^2)$	$(1 + e^{-i\pi\alpha_\sigma})/2$	-0.17	14.6
f_2	$0.9(t - m_{f_2}^2) + 2$	$(1 + e^{-i\pi\alpha_{f_2}})/2$	0.0376	6.45; 0.0
f_1	$0.028t + 0.9$	$(-1 + e^{-i\pi\alpha_{f_1}})/2$	0.18	2.5

photon-like quantum number $J^{PC} = 1^{-+}$ in the ω photoproduction plays the role unique in the slow increase of cross sections up to $\sqrt{s} \approx 100$ GeV. We use the trajectory $\alpha_\mathbb{P}(t) = 0.25t + 1.08$ and the decay constant $f_\omega = 15.6$ from the SU(3) symmetry,

$$\frac{1}{f_\rho} : \frac{1}{f_\omega} : \frac{1}{f_\phi} = 3 : 1 : -\sqrt{2}, \quad (10)$$

which is consistent with $f_\phi = -13.4$ [6] and $f_\rho = 5.2 = 2g_{\rho NN}$ [23]. The parameters for the quark-Pomeron coupling are given by $\beta_u = \beta_d = 2.07$ GeV $^{-1}$, and the cutoff mass $\mu_0^2 = 1.1$ GeV 2 . We adopt the nucleon isoscalar form factor $F_1(t)$ as given in Ref. [6].

Unnatural parity exchange

- Pion $J^{PC} = 0^{-+}$

To determine the contribution of π exchange is important, because it is crucial to characterize the overall feature of reaction in the low energy region. The coupling constants $g_{\pi NN} = \pm 13.4$ are used for the γp and γn reactions, respectively, and $|g_{\gamma \pi \omega}| = 0.69$ from the radiative decay width $\Gamma_{\omega \rightarrow \gamma \pi} = 0.7$ MeV reported in the PDG. However, it is not easy to determine the sign of the radiative coupling from the unnatural parity cross section, because of the single dominance of π exchange over the contribution of f_1 exchange which is negligible. In this work we choose the negative sign of $g_{\gamma \pi \omega}$ for a fair agreement with experimental data. In the reggeization, the phase of π exchange takes the canonical form, because the exchange-degenerate partner b_1 of negative C -parity is absent from the reaction. Nevertheless, we take the complex phase for the γp reaction, which is consistent with the scaled differential cross section as will be discussed later. For the γn reaction we take the constant phase for the π Reggeon to agree with differential cross sections of Ref. [9].

- $f_1(1285) J^{PC} = 1^{++}$

Together with the pseudoscalar π exchange the exchange of axial vector meson constitutes the contribution

from the unnatural parity. However, the case of a_1 exchange is excluded because it does decay to neither $V\gamma$ nor $\gamma\gamma$ decay, while the f_1 is possible to decay via both channels. As for the reggeization of f_1 , a special form of the trajectory $\alpha_{f_1}(t) = 0.028t + 0.9$ is suggested in Ref. [24], which is deduced from QCD axial anomaly. In the $\gamma p \rightarrow \phi p$ reaction we found it to contribute at high energies with the flat slope and positive intercept comparable to those of Pomeron [6]. With an expectation of such a special role at high energy, we include f_1 exchange in the present model. We use the coupling constant $g_{f_1 NN} = 2.5$ [6]. However, since the decay width $f_1 \rightarrow \omega\gamma$ is not measured yet, we refer to theoretical estimates such as the constituent quark model [21] where the partial decay widths are estimated as $\Gamma_{f_1 \rightarrow \rho^0 \gamma} = 509$ keV, $\Gamma_{f_1 \rightarrow \omega \gamma} = 48$ keV, and $\Gamma_{f_1 \rightarrow \phi \gamma} = 20$ keV, respectively. These are comparable to the values 675 keV for the $f_1 \rightarrow \rho^0 \gamma$ estimated from the fraction $(2.8 \pm 0.7) \times 10^{-2}$ [25] to the full width $\Gamma_{f_1} = 24.1$ MeV, and 18.1 keV for the $f_1 \rightarrow \phi \gamma$ reported in the PDG. Thus, we adopt the estimate above to obtain $g_{\gamma f_1 \omega} = 0.18$. The nucleon axial form factor is taken the same as in Ref. [26] with the cutoff mass $M_A = 1.08$ GeV for the sake of consistency.

Before proceeding, we give a few comments on the t -channel exchanges. Here we neglect the pseudoscalar meson η exchange for simplicity, because its contribution is suppressed by the larger mass and the smaller branching ratio $\omega \rightarrow \eta\gamma$ in comparison to π exchange. For the spin-2 tensor meson, a_2 meson could contribute as well in the isovector channel. However, the determination of $g_{\gamma a_2 \omega}$ is somewhat confusing because the constituent quark model [21] predicts the decay width $\Gamma_{a_2 \rightarrow \omega \gamma} = 247$ keV which leads to $g_{\gamma a_2 \omega} = 0.1$. It is larger than $g_{\gamma f_2 \omega}$ by a factor of 2.7, although the decay $\Gamma_{a_2 \rightarrow \gamma \gamma} = (9.4 \pm 0.7) \times 10^{-6}$ is less than $\Gamma_{f_2 \rightarrow \gamma \gamma} = (1.64 \pm 0.19) \times 10^{-5}$ by a factor of 1.74 from the PDG. For a reasonable choice, in favor of the two gamma decays based on the vector meson dominance, we rather assume that the decay $\Gamma_{a_2 \rightarrow \omega \gamma}$ is similar to $\Gamma_{f_2 \rightarrow \omega \gamma}$ in magnitude at best and take the decay width $\Gamma_{a_2 \rightarrow \omega \gamma} = 26$ keV to obtain $g_{\gamma a_2 \omega}/m_0 = 0.033/m_0$. With $g_{a_2 NN}^{(1)} = 1.4$ and $g_{a_2 NN}^{(2)} = 0$ chosen [22], its contribution turns out to be in minor role, which is less than that of f_2 by a factor of 10^{-2} order. We, thus, exclude it for simplicity.

We summarize the coupling constants and trajectories with the corresponding phase factors in Table I.

B. Regge cuts

Figure 1 shows the natural and unnatural parity cross sections, σ^N and σ^U , respectively [8]. In (a) the solid and dashed curves correspond to the cross section with and without σ exchange. This signifies the role of σ exchange indispensable as the peaking of cross section σ^N near threshold cannot be reproduced without it.

The case for the unnatural parity is shown in (b) where the dashed curve is the cross section from the pure π

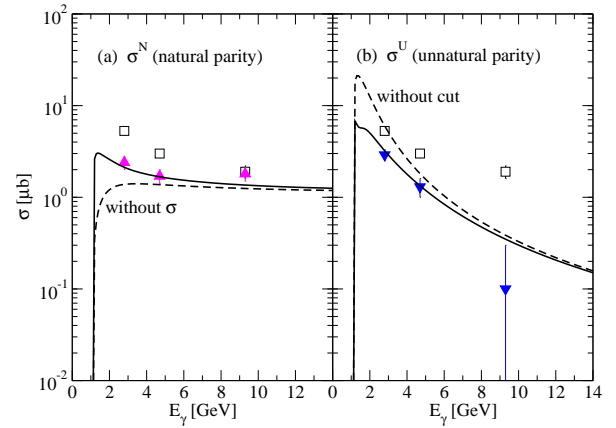


FIG. 1. Natural and unnatural parity cross sections, σ^N and σ^U , for $\gamma p \rightarrow \omega p$. In (a) solid and dashed curves are with and without σ meson exchange. In (b) solid and dashed curves are with and without the cuts in the unnatural parity cross section. Empty squares are the data of total cross section. Data are taken from Ref. [8].

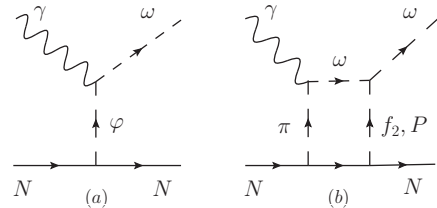


FIG. 2. Reggeons $\varphi = \pi, \sigma, f_2$ (a) and absorptive cuts in the exclusive $\gamma N \rightarrow \omega N$ process at forward angles (b). Elastic cuts π - f_2 and π - P are viewed as the exchange of two Reggeons.

exchange. Thus, without any sort of reduction, the exchange of π Reggeon should overestimate the data by a factor of two as shown in Fig. 1(b). On the other hand, the contribution of η meson exchange of the same parity is too small to improve the overdominance of the π exchange only by the coupling constants $g_{\gamma \eta \omega} = 0.161$ and $g_{\eta NN} = 3.53$ [17]. In order to modulate such a strong contribution of the π exchange we need to introduce the Regge-cuts [27] which are relevant to the Regge formulation of the production amplitude rather than the form factors with cutoff masses. The cuts are caused by absorption effects due to the elastic scattering $\omega N \rightarrow \omega N$ through the sequential subprocess as shown in Fig. 2(b).

For the couplings allowed for the $\omega N \rightarrow \omega N$ subprocess in the elastic cut, isoscalar mesons σ and f_2 in addition to the Pomeron exchange could be a candidate. Then, the cuts are effective in the unnatural parity channel because the overall naturality of the t -channel exchange in Fig. 2 (b) is unnatural by the product of pion naturality and the natural parity exchanges of the mentioned mesons. In the calculation we neglect σ for the small intercept of π - σ cut in comparison to others, and write the π Reggeon amplitude by extending Eq. (6) to

TABLE II. Cut parameters C_φ and d_φ given in units GeV^{-2} .

Reaction	Cut	C_φ	d_φ
γp	$\pi-f_2$	41	2.2
	$\pi-\mathbb{P}$	-2.5	2
γn	$\pi-f_2$	11.5	2.2
	$\pi-\mathbb{P}$	6	2

include the cuts as,

$$\mathcal{M}_\pi^{\text{cut}} = \widetilde{\mathcal{M}}_\pi \left[\mathcal{R}^\pi(s, t) + \sum_{\varphi=f_2, \mathbb{P}} C_\varphi e^{d_\varphi t} e^{-i\frac{\pi}{2}\alpha_{\pi\varphi}(t)} \left(\frac{s}{s_0} \right)^{\alpha_{\pi\varphi}(t)-1} \right], \quad (11)$$

with the φ stands for f_2 and \mathbb{P} in Fig. 2 (b). Here the $\widetilde{\mathcal{M}}_\pi$ denotes the pion interaction vertices in Eq. (6) excluding the Reggeon \mathcal{R}^π . C_φ is the strength of the cut and d_φ is the parameter for the range of the π - φ cut to be fitted to data. Both parameters have the dimension of GeV^{-2} . The trajectory of the π - φ cut in Eq. (11) is determined by the combination of π and φ meson trajectories which is given by

$$\alpha_{\pi\varphi}(t) = \alpha'_{\pi\varphi} t + \alpha_{\pi\varphi}^0 \quad (12)$$

with

$$\alpha'_{\pi\varphi} = \frac{\alpha'_\pi \alpha'_\varphi}{\alpha'_\pi + \alpha'_\varphi}, \quad \alpha_{\pi\varphi}^0 = \alpha_\pi(0) + \alpha_\varphi(0) - 1 \quad (13)$$

for $\varphi = f_2, \mathbb{P}$, respectively. With the parameters C_φ and d_φ in the cuts summarized in Table II we present the solid curve which agrees with the unnatural parity cross section for γp reaction in Fig. 1 (b). On the other hand, the C_φ and d_φ for the γn Reaction in Table II are fitted to the differential and total cross sections.

III. RESULTS

A. $\gamma p \rightarrow \omega p$

Differential and total cross sections

The t -dependence of differential cross sections are presented in Fig. 3 in four energy bins which are selected to represent the energy region at threshold, intermediate, and high energy, respectively. The overestimate of the single π exchange without cuts is shown by the dotted curve at $E_\gamma = 1.475$ GeV. The contribution of π exchange modulated by the absorptive cuts gives a fair agreement with differential cross sections. The role of f_1 exchange with the flat slope and large intercept for the trajectory appears to raise up the cross section at high energies $70 < \sqrt{s} < 90$ GeV.

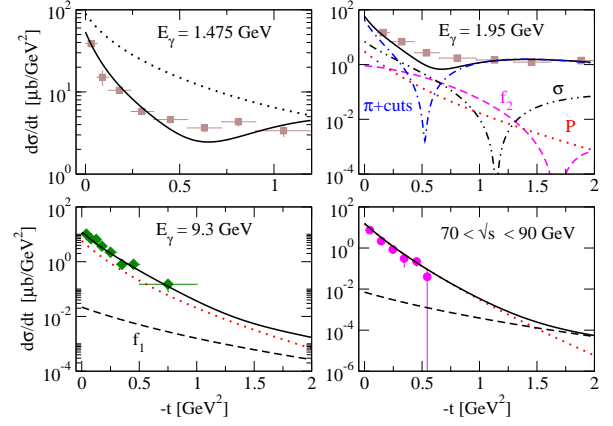


FIG. 3. Differential cross sections for $\gamma p \rightarrow \omega p$ in four energy bins. Data are taken from Refs. [8, 9, 28]. Solid curves are from the full calculation. Dotted, dashed, dash-dotted, and dash-dot-dotted curves are the contributions of Pomeron, f_2 , π +cuts, and σ meson exchanges, respectively.

Total cross section for $\gamma p \rightarrow \omega p$ is shown in Fig. 4 with the energy dependence from threshold $\sqrt{s} \approx 1.72$ GeV up to the realm of the Pomeron exchange. At high energies, the Pomeron exchange is dominant and the data are well reproduced by the single Pomeron exchange. Note that the π exchange without the cuts would make an overestimate of the peak of the cross section near threshold. The cross section in intermediate energies is sustained by the f_2 and Pomeron exchanges.

Density matrix and Beam polarization asymmetry

Spin density matrix elements ρ_{ij}^a are important observables because they are related with the single spin polarizations such as the parity and beam polarization asymmetries. The parity asymmetry P provides information

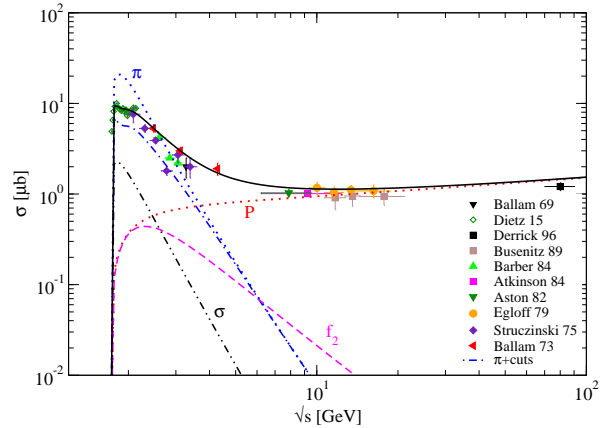


FIG. 4. Total cross section for $\gamma p \rightarrow \omega p$. Data are taken from Refs. [8, 9, 14, 28–34]. Notations for the curves are the same as in Fig. 3.

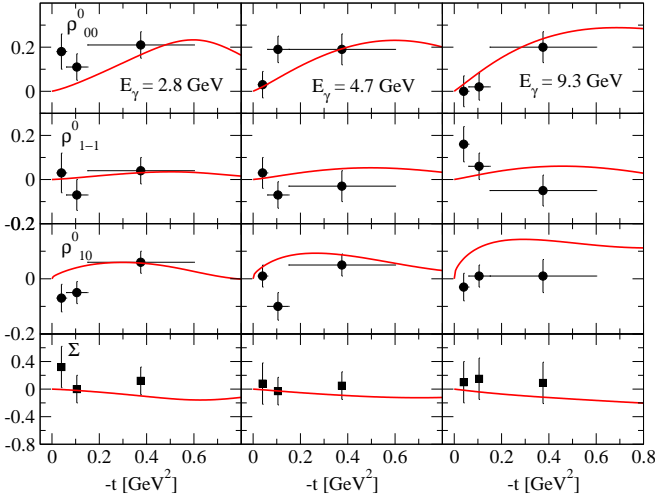


FIG. 5. Spin-density matrix elements, parity and beam polarization asymmetries in the Gottfried-Jackson frame for $\gamma p \rightarrow \omega p$ at $E_\gamma = 2.8, 4.7$ and 9.3 GeV. Data are taken from Ref [8]. Beam polarization asymmetry is obtained from spin density matrix elements via using Eq. (15).

on the naturality of the reaction which is defined as

$$P_\sigma = 2\rho_{1-1}^1 - \rho_{00}^1 \quad (14)$$

in the Gottfried-Jackson frame. Furthermore, as the beam polarization Σ is one of important observables for the study of recent JLab GlueX data we list it by extracting it from the spin density matrix elements in Eq. (15) below.

The beam polarization in the Gottfried-Jackson frame is defined as [35]

$$\Sigma = 2\rho_{11}^1 + \rho_{00}^1, \quad (15)$$

with the trace condition $\sum_i \rho_{ii}^0 = 1$. Figure 5 shows a qualitative agreement of the spin density matrix elements, parity asymmetry, and beam polarization asymmetry with the data over the resonance region, $E_\gamma = 2.8, 4.7$ and 9.3 GeV [8]. We note that the prediction of P_σ is of the same quality as that of Ref. [35]. The $P_\sigma \approx 1$ at $E_\gamma = 9.3$ GeV implies that the reaction proceeds via the natural parity exchange by its definition $P_\sigma = \frac{d\sigma^N - d\sigma^U}{d\sigma^N + d\sigma^U}$. The vanishing of Σ over the resonance region is a feature from the pure meson exchanges. Nevertheless, our model fails to predict the beam polarization and the double polarization at low energies such as beam-target in the low energy region recently measured at the CBELSA/TAPS [9, 36]. As pointed out in previous work [37] the contribution of N^* resonances in the s -channel is essential in order to reproduce the observed spin polarizations negative and nonvanishing at low energy, which is, however, beyond the scope of the present work.

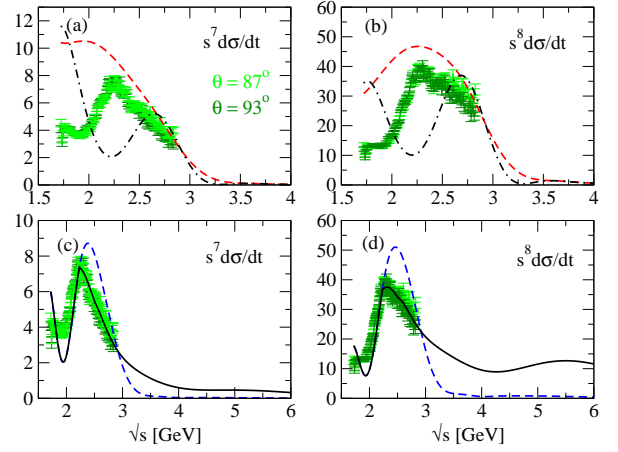


FIG. 6. Differential cross sections for $\gamma p \rightarrow \omega p$ at $\theta = 90^\circ$ scaled by s^7 and s^8 in units of $10^7 \text{ GeV}^{12} \text{ nb}$ and $10^7 \text{ GeV}^{14} \text{ nb}$, respectively. By using the linear trajectories the sensitivity of the cross section to cuts as well as the phase of the π exchange is investigated in (a) for s^7 and (b) for s^8 scaled cross sections. Dashed curves are from the full calculation where the complex phase is taken for the π exchange without cuts, whereas the dash-dotted are from π exchange with cuts but canonical phase, $(1 + e^{-i\pi\alpha_\pi})/2$, respectively. Nonlinearity of trajectory is tested in (c) and (d). Given the π exchange with complex phase and cuts, solid curves result from trajectories of π , σ , and f_2 saturated as shown in Fig. 7 (a), whereas the dashed ones are the results without saturation. Data are taken from Ref. [40].

Scaling at large angle

By the quark counting rule the energy dependence of differential cross section obeys the power-law scaling, i.e.,

$$s^{n-2} \frac{d\sigma}{dt} \sim F(\theta), \quad (16)$$

at the angle θ in the center of mass system. Thus, a direct photon coupling leads to $n = 9$, whereas the vector meson dominance needs $n = 10$, respectively. These are expected to exhibit a scaling either by the factor of s^7 , or by s^8 as the reaction energy increase. Therefore, a precise measurement of the cross section around $\theta = 90^\circ$ could provide us a criterion to decide what portion of photon could convert to a vector meson propagating as an effective degree of freedom.

For the saturation of a linear trajectory $\alpha(t)$ we use a simple parameterization of the square root function [38]

$$\alpha^*(t) = c_1 + c_2 \sqrt{t_1 - t}, \quad (17)$$

where the coefficients c_1 and c_2 are determined by the boundary conditions $\alpha^*(t_0) = \alpha(t_0)$ and $d\alpha^*(t_0)/dt = d\alpha(t_0)/dt$ at the saturation point t_0 where we choose to make the trajectory saturating to -1 . Then, t_1 is the initial point of the square root function the argument of which should be positive and we take as $t_1 > t_0$ in the calculation.

We now discuss the application of the present model to the scaled cross sections at large $-t$. For doing this we consider the saturation of a trajectory as $-t \rightarrow \infty$, in which case the trajectory becomes independent of t , as a result [38, 39].

For the sake of consistency, the nonlinear trajectory given by Eq. (17) is applied to the cut trajectories for π - f_2 and π - \mathbb{P} as well. Nevertheless, this does not expect to affect the previous results because the cuts are by themselves effective for the very small $-t$. The slopes and intercepts of the π - f_2 cut trajectory in Eq. (12) are, therefore, parameterized as

$$\alpha'_{\pi f_2} = \frac{\alpha'^*_{\pi} \alpha'^*_{f_2}}{\alpha'^*_{\pi} + \alpha'^*_{f_2}}, \quad \alpha^0_{\pi f_2} = \alpha^*_{\pi}(0) + \alpha^*_{f_2}(0) - 1, \quad (18)$$

in Eq. (13) with the starred quantities taken to be the slope and intercept of Reggeon trajectory nonlinearized by Eq. (17). However, in consideration of the characteristics of the Pomeron exchange at the very forward angle we keep the Pomeron trajectory unsaturated, while taking the nonlinear π trajectory in the cut so that

$$\alpha'_{\pi \mathbb{P}} = \frac{\alpha'^*_{\pi} \alpha'_{\mathbb{P}}}{\alpha'^*_{\pi} + \alpha'_{\mathbb{P}}}, \quad \alpha^0_{\pi \mathbb{P}} = \alpha^*_{\pi}(0) + \alpha_{\mathbb{P}}(0) - 1, \quad (19)$$

for the π - \mathbb{P} cut.

Figure 6 shows predictions for scaled differential cross sections for the γp reaction with the saturation of trajectories by choosing $t_0 = -1.325$, $t_1 = -0.85$ for π , by $t_0 = -1.0$, $t_1 = -0.95$ for σ , and by $t_0 = -2.0$, $t_1 = -1.5$ for f_2 in unit of GeV^2 . The data are collected from the measurement at $\theta = 87^\circ$ and 93° by the CLAS Collaboration [40] and re-sorted to the cross sections $s^7 d\sigma/dt$ and $s^8 d\sigma/dt$, respectively. With the trajectories unsaturated, we first examine the sensitivity of the cross sections to the cuts and phase of π exchange in (a) and (b). In lower row (c) and (d) we note that the saturation of trajectories at mid angle is significant and suggestive of nonvanishing

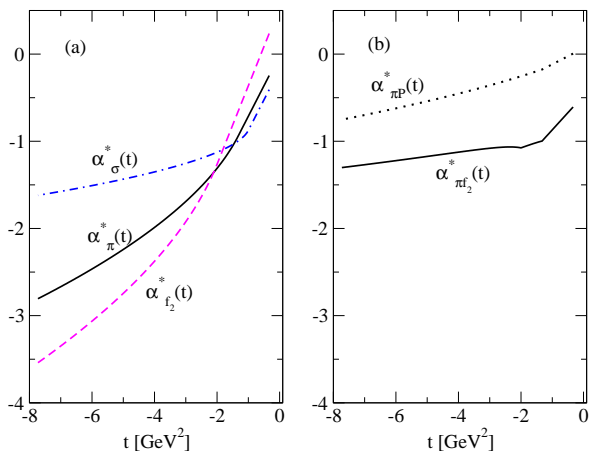


FIG. 7. Saturation of trajectories for Reggeons (a) and cuts (b).

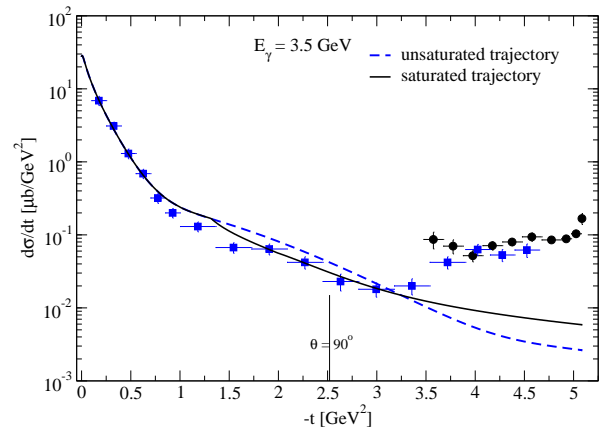


FIG. 8. Differential cross section for $\gamma p \rightarrow \omega p$ as a function of $-t$. Nonlinear trajectories agree with data around $\theta = 90^\circ$ with a limit of meson exchange model appearing at the very backward angles. Data are taken from Refs. [41, 42].

data, respectively. In Fig. 7, we show the nonlinear behavior of Reggeon and cut trajectories with respect to momentum squared t . In order for an agreement with data as shown in Fig. 6 (c) and (d) we have to make the saturation of the trajectories in Fig. 7 (a) to have a smooth decrease of the t dependence rather than a strict approach to an ideal limit -1 .

The dependence of differential cross section on the momentum squared $-t$ is reproduced at $E_\gamma = 3.5 \text{ GeV}$ with the nonlinear trajectories and compared to the case without saturation in Fig. 8. Around $\theta \approx 90^\circ$ the cross section from the nonlinear trajectories is in good agreement with existing data, though a limit of the t -channel Regge model to the very backward angles $-t > 3.5 \text{ GeV}^2$ appears as a large discrepancy with data. The rise of data over $-t \approx 3.5 \text{ GeV}^2$ could be further accounted for by the u -channel nucleon Reggeon, and a comprehensive description of the backward process which could cover up this issue will appear elsewhere.

Before closing the application of the nonlinear trajectory to the scaling of ω photoproduction at wide angles, a few remarks should be in order. First, we observe that the absorptive cuts play the role not only important to reduce the strength of the π exchange but also crucial to reproduce the scaled differential cross section. At second, the canonical phase $(1 + e^{-i\pi\alpha_\pi})/2$ is not valid to reproduce the scaled cross section as shown in Fig. 6, because it leads to a minimum at the nonsense zeros of the phase, i.e., $1 + e^{-i\pi\alpha_\pi} = 0$, which is opposite to the peak of the cross section $s^7 d\sigma/dt$ observed at $\sqrt{s} \simeq 2.27$. Furthermore, as in Fig. 6(a) and (b), such a phase yields the dips in the differential cross section which are not seen in the experimental data. These support the complex phase for the π Reggeon as adopted in Table I. Lastly, both the s^7 and s^8 scaled cross sections in Fig. 6(c) and (d) show nonzero cross sections ≈ 0.3 and 10 in their respective sizes over $\sqrt{s} \approx 3 \text{ GeV}$, i.e., a *genuine* scaling through the hard process. Otherwise, they are vanishing

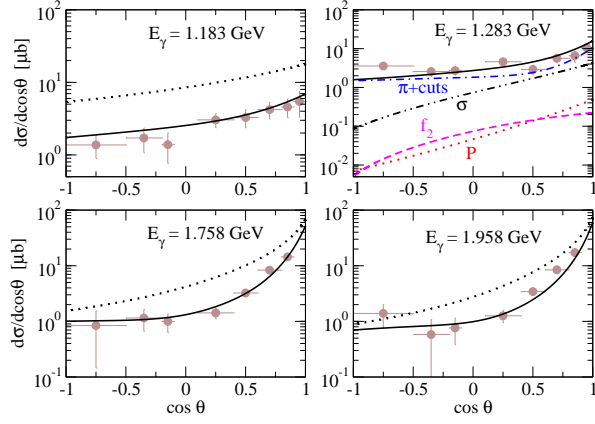


FIG. 9. Differential cross sections for $\gamma n \rightarrow \omega n$. Dotted curves are the cross sections without cuts. Dashed-dotted, dash-dot-dotted, and dashed curves are from π exchange with cuts, σ , and f_2 exchanges, respectively. Pomeron exchange is given by the red dotted curve. Data are taken from Ref. [9].

with the linear trajectories. Moreover, noticing that the relative size between s^7 and s^8 cross section is $\approx 1/5$ below $\sqrt{s} \approx 3$ GeV, and finding that it is further reduced to $\approx 1/30$ in the scaling region as above, we expect that this give us a clue to discern which one is probable between the direct photon coupling and the vector meson dominance, if data exit beyond $E_\gamma = 3$ GeV further. Therefore, a measurement of the cross section at $\theta = 90^\circ$ extending to a region over $\sqrt{s} \approx 3$ GeV is highly desirable.

B. $\gamma n \rightarrow \omega n$

Differential and total cross sections

Experimental data on the γn reaction are not enough to investigate the reaction mechanism up to high energy, and the data recently measured at the CBELSA/TAPS Collaboration [9] are restricted only to a lower energy region. In this subsection we calculate the energy and angle dependences of the γn reaction to provide differential and total cross sections to compare with data available.

In the photoproduction amplitude the only difference between γp and γn reactions is the contribution of isovector π exchange with the sign of $g_{\pi nn}$ opposite to $g_{\pi pp}$, as listed in Table I. Within the present framework we further modify the cut parameters and change the phase of π exchange to obtain an agreement with differential and total cross sections.

Differential cross sections in the resonance region are reproduced in Fig. 9 where the constant phase of π Reggeon is taken to reproduce the CBELSA/TAPS data. The respective contributions of meson exchanges are shown at $E_\gamma = 1.283$ GeV.

Figure 10 shows the total cross section for γn reaction at low energy with the data from the quasi-free neutron

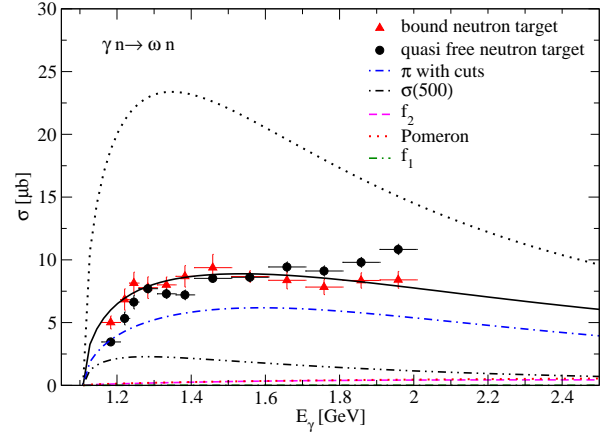


FIG. 10. Total cross section for $\gamma n \rightarrow \omega n$. Solid curve is the cross section from the full calculation with the cuts included in the π exchange. Cross section without the cuts is shown by dotted curve which is wide out of data. Data are taken from Ref. [9].

and bound neutron in the deuteron targets, respectively. The cut parameters in Table II are fixed to reproduce the total cross section of the reaction with the bound neutron in the final state. As shown in the figure, the role of the cuts in the γn reaction is crucial to agree with experiment as well.

C. Application to $\omega\Delta$ photoproduction

In this subsection we discuss the analysis of $\gamma p \rightarrow \omega\Delta^+$ basically in the same framework as described above for the ω photoproduction on nucleon, but the Dirac spinor for the nucleon is replaced by the Rarita-Schwinger spinor for the spin-3/2 Δ baryon in the final state. The experimental data for the differential cross sections at $E_\gamma = 2.8$ - 4.8 GeV and the corresponding data points in the total cross section were measured by the LAMP2 Group [14]. More recent experiment of the reaction is performed by the CB-ELSA Collaboration in which case the differential and total cross sections were measured below $E_\gamma = 3$ GeV [15]. In Ref. [16] the Regge pole model was applied for the $\gamma p \rightarrow \omega\Delta^+$ to discuss the nondiffractive feature of the reaction with the conclusive results from the role of the π exchange primarily with cuts but the tensor meson a_2 in minor role.

Here we pay our attention to the production mechanism rather in the higher energy beyond $E_\gamma = 3$ GeV because the data points of the total cross section below the energy from the CB-ELSA Collaboration are scattered. For the $\gamma p \rightarrow \omega\Delta^+$ process only the isovector exchange is allowed in the t -channel by the transition of isospin 1/2 proton to the 3/2 Δ^+ . Thus, neither the Pomeron nor the isoscalar mesons σ and f_2 are exchanged in the reaction process. In this work we consider the π exchange

which is expected to give the leading contribution with the large decay width $\omega \rightarrow \pi\gamma$. For the test of the Regge pole fit to data [16], we also include the a_2 exchange.

Pion exchange in the t -channel is gauge-invariant by itself with the production amplitude given as,

$$\mathcal{M}_\pi = -i \frac{g_{\gamma\pi\omega}}{m_0} \frac{f_{\pi N\Delta}}{m_\pi} \varepsilon_{\mu\nu\alpha\beta} \epsilon^\mu \eta^{*\nu} k^\alpha Q^\beta \times \bar{u}_\lambda(p') Q^\lambda u(p) \mathcal{R}^\pi(s, t) \quad (20)$$

with the coupling constant $g_{\gamma\pi\omega}$ from Table I. The spin-3/2 spinor is denoted by u_λ . The determination of the coupling constant π exchange is of importance because it gives the most dominant contribution to the process. From the empirical value for the maximum width $\Gamma_{\Delta \rightarrow \pi N} = 120$ MeV taken from PDG, the $\pi N\Delta$ coupling constant is estimated to be $f_{\pi^- p \Delta^{++}} \approx 2.16$. According to the $\pi N\Delta$ transition based on the quark model wave function, the $\pi N\Delta$ coupling reads [43],

$$f_{\pi N\Delta} = \frac{6\sqrt{2}}{5} f_{\pi pp} \quad (21)$$

which gives $f_{\pi N\Delta} \approx 1.70$ with $f_{\pi pp} = 1.0$ taken. Therefore, we consider $f_{\pi N\Delta}$ in the range $1.7 \leq f_{\pi N\Delta} \leq 2.16$ to take 1.7 for a consistency with the quark model prediction.

For tensor meson $T (= a_2)$ exchange we assume a simple form for the $TN\Delta$ from the TNN vertex [44] in consideration of parity and spin, i.e.,

$$\bar{u}(p') (\gamma_\sigma P_\lambda + \gamma_\lambda P_\sigma) u(p) e^{\sigma\lambda} \rightarrow \bar{u}'(p') (g_{\nu\sigma} P_\lambda + g_{\nu\lambda} P_\sigma) \gamma_5 u(p) e^{\sigma\lambda} \quad (22)$$

with $e^{\sigma\lambda}$ representing the spin polarization tensor of tensor meson a_2 .

The production amplitude reads

$$\begin{aligned} \mathcal{M}_{a_2} &= \bar{u}^\lambda(p') \\ &\times \frac{4g_{\gamma a_2 \omega}}{m_0} [(k \cdot q \epsilon_\beta - \epsilon \cdot q k_\beta) \eta_\rho + (\epsilon \cdot \eta k_\beta - k \cdot \eta \epsilon_\beta) q_\rho] \\ &\times \Pi^{\beta\rho; \sigma\lambda}(Q) \frac{f_{a_2 N\Delta}}{m_{a_2}} \bar{u}'(p') (g_{\nu\sigma} P_\lambda + g_{\nu\lambda} P_\sigma) \gamma_5 u(p) \mathcal{R}^{a_2}, \end{aligned} \quad (23)$$

where $P = (p + p')/2$ and spin-2 projection $\Pi^{\beta\rho; \sigma\lambda}(Q)$ given in Eq. (9). We use the trajectory $\alpha_{a_2}(t) = 0.9(t - m_{a_2}^2) + 2$ and the coupling constant $\frac{f_{a_2 N\Delta}}{m_{a_2}} \approx -3 \frac{f_{\rho N\Delta}}{m_\rho}$ following the t -channel helicity Regge-pole fit to data in Ref. [16, 45]. For the relation above we adopt $f_{\rho N\Delta} = 8.57$ [46]. The radiative coupling constant is taken to be $g_{\gamma a_2 \omega}/m_0 = 0.033/m_0$, as discussed in Sec. II A.

In consideration of isospin relations [16] we now write the production amplitude as

$$\mathcal{M}(\gamma p \rightarrow \omega \Delta^+) = \sqrt{\frac{2}{3}} [\mathcal{M}_\pi^{\text{cut}} + \mathcal{M}_{a_2}], \quad (24)$$

where the $\mathcal{M}_\pi^{\text{cut}}$ includes the elastic cut of the same form as in Eq. (11) for the π - a_2 exchanges with the cut parameters $C_{a_2} = 4 \text{ GeV}^{-2}$ and $d_{a_2} = 1.5 \text{ GeV}^{-2}$ chosen.

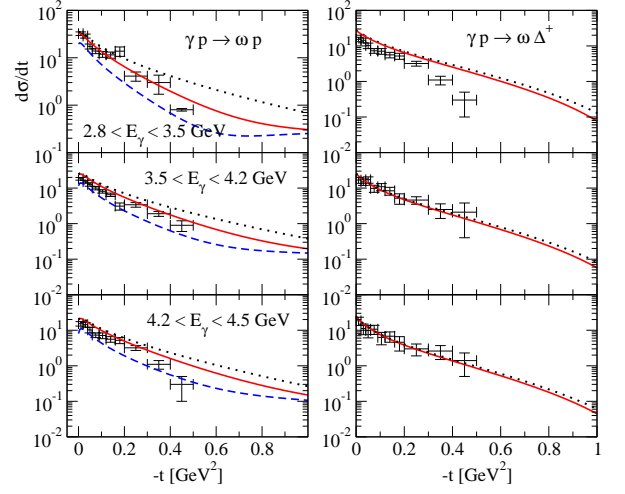


FIG. 11. Comparison of differential cross sections between $\gamma p \rightarrow \omega p$ and $\gamma p \rightarrow \omega \Delta^+$ photoproductions. In both reactions the solid and dotted curves show the cross sections with and without cuts, respectively. The dashed curve in the left panel denotes the π contribution with cuts. Data are taken from

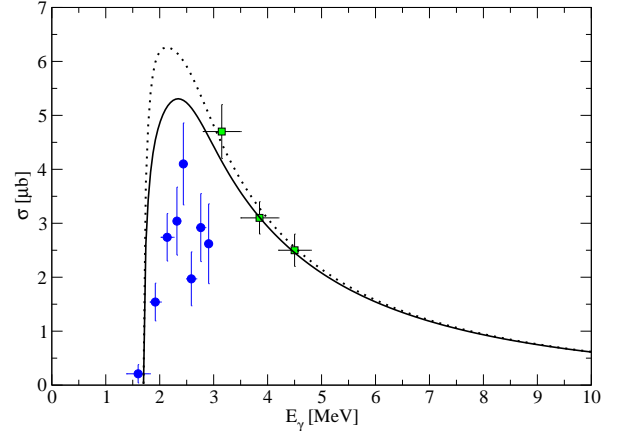


FIG. 12. Total cross section for $\gamma p \rightarrow \omega \Delta^+$. Solid and dotted curves are the cross sections with and without the cut. Data are taken from Refs. [14, 15].

In the calculation the phase of the canonical form, $(1 + e^{-i\pi\alpha(t)})/2$, is taken for the π and a_2 mesons in Eq. (24). Numerical consequences in the differential cross sections are presented in Fig. 11 where the $\gamma p \rightarrow \omega \Delta^+$ reaction is compared with the $\gamma p \rightarrow \omega p$ reaction. It is shown that most of the contribution comes from the π exchange in both processes. However, in contrast to the $\gamma p \rightarrow \omega p$ reaction the role of the π - a_2 cut is not quite clear in the case of $\gamma p \rightarrow \omega \Delta^+$ as can be seen in the differential and total cross sections in Figs. 11 and 12. The present model with the production amplitude in Eq. (24) predicts a good agreement with the differential cross section data

at $E_\gamma = 8.9$ GeV in Ref. [16]. Nevertheless in order to clarify the cut effect on this reaction more data with precision should be measured for the total cross section below $E_\gamma = 3$ GeV. The maximum contributions of the $a_2(1320)$ exchange is found to be of 10^{-2} order in the total cross section so that the differential and total cross sections are completely reproduced by the π exchange alone. The a_2 exchange found in minor role is consistent with the observation of Ref. [16].

IV. SUMMARY AND CONCLUSIONS

In summary we have investigated photoproduction of ω off a nucleon target from threshold up to invariant energy $\sqrt{s} \approx 100$ GeV within the Regge framework for $\sigma + f_2 + \mathbb{P} + \pi + f_1$ exchanges. The roles of these mesons are fixed by the consistency with the natural and unnatural parity cross sections independently. Cross sections for differential, total, spin density matrix and beam polarization are reproduced to explain existing data on the reaction $\gamma p \rightarrow \omega p$. Scaled differential cross sections for $\gamma p \rightarrow \omega p$ are analyzed at the production angle $\theta = 90^\circ$ with the saturation of trajectories substantial to agree with Jefferson Lab data. Differential and total cross sections for the $\gamma n \rightarrow \omega n$ reaction are analyzed to compare with recent experimental data at the CBELSA/TAPS Collaboration. The most prominent feature of ω photoproduction at low energies comes from the strong contribution of π exchange together with absorptive cuts. Need of σ meson exchange is demonstrated in reproducing the natural parity cross section. At high energies where the Pomeron exchange prevails, the f_1 exchange plays the role to raise the cross section in the large $-t$ as expected from the trajectory specialized by the QCD anomaly. But its role in the reaction at low energy is much suppressed in comparison to others. These characterize the features of $\gamma N \rightarrow \omega N$ reaction for small $-t$, as viewed from the t -channel Reggeon exchange. Analysis of scaled differential cross section is particularly interest-

ing, because it further supports the validity of the cuts as well as the complex phase of the π exchange both of which are substantial to explain experimental data. Non-linear trajectories from a simple square root function are considered for the saturation of the Reggeons and applied to describe the reaction at large $-t$. Scaled cross sections by s^7 or s^8 at $\theta = 90^\circ$ are found to agree with existing data, respectively, below $\sqrt{s} \approx 3$ GeV. Nevertheless, they are predicted to behave different scaling over $\sqrt{s} \approx 3$ GeV from each other, which could be a clue to distinguish the priority between the direct photon coupling and vector meson dominance. In this respect, we hope that in future experiments there should be a measurement of differential cross sections around mid angle in the discussed region so that we could ask how parton contributions arise there.

The leading role of the π exchange continues at the $\gamma p \rightarrow \omega \Delta^+$ reaction. However the role of the πa_2 cut is found to be insignificant and the reaction is completely dominated by the single π exchange up to $E_\gamma = 9$ GeV. Therefore, it is concluded that the production mechanism of the $\gamma p \rightarrow \omega \Delta^+$ process by the single π exchange of the unnatural parity is quite different from that of the $\gamma p \rightarrow \omega p$ process in which case the isoscalar $\sigma + f_2 + \text{Pomeron}$ exchanges of the natural parity play a role up to high energies.

It is expected that the theoretical structures of the $\gamma p \rightarrow \omega p$ and $\gamma p \rightarrow \omega \Delta^+$ photoproductions we provided in this work will help understanding not only the reaction mechanisms themselves but also the vector meson properties in the nuclear medium in future experiments.

ACKNOWLEDGMENTS

This work was supported by the grant NRF-2017R1A2B4010117, and partly by the grant NRF-2013M7A1A1075764 from National Research Foundation (NRF) of Korea.

-
- [1] J.-M. Laget, Phys. Lett. B **489**, 313 (2000).
 - [2] B. Friman and M. Soyeur, Nucl. Phys. A **600**, 477 (1996).
 - [3] E. Chudakov, S. Gevorkyan, and A. Somov, Phys. Rev. C **93**, 015203 (2016).
 - [4] A. Sibirtsev, Ch. Elster, J. Speth, arXiv:nucl-th/0203044.
 - [5] A. Sibirtsev, K. Tsushima, S. Krewald, Phys. Rev. C **67**, 055201 (2003).
 - [6] B.-G. Yu, H. Kim, K.-J. Kong, Phys. Rev. D **95**, 014020 (2017).
 - [7] F. Cano, J.-M. Laget, Phys. Rev. D **65**, 074022 (2002).
 - [8] J. Ballam, G. B. Chadwick, Y. Eisenberg, E. Kogan, K. C. Moffeit, P. Seyboth, I. O. Skillicorn, H. Spitzer, G. Wolf, H. H. Bingham, W. B. Fretter, W. J. Podolsky, M. S. Rabin, A. H. Rosenfeld, and G. Smadja, Phys. Rev. D **7**, 3150 (1973).
 - [9] F. Dietz *et al.* (CBELSA/TAPS Collaboration), Eur. Phys. A **51**, 6 (2015).
 - [10] A. Wilson *et al.* (CBELSA/TAPS Collaboration), Phys. Lett. B **749**, 407 (2015).
 - [11] S. J. Brodsky and G. R. Farrar, Phys. Rev. Lett. **31**, 1153 (1973).
 - [12] L. Y. Zhu *et al.* (Jefferson Lab Hall A Collaboration) Phys. Rev. C **71**, 044603 (2005).
 - [13] B. Dey, Phys. Rev. D **90**, 014013 (2014).
 - [14] D. P. Barber *et al.*, Z. Phys. C **26**, 343 (1984).
 - [15] J. Junkersfeld *et al.* (CB-ELSA Collaboration), Eur. Phys. J. A **31**, 365 (2007).
 - [16] M. Clark and A. Donnachie, Nuclear Materials B **125**, 493 (1977).
 - [17] A. I. Titov and T.-S. H. Lee, Phys. Rev. C **66**, 015204 (2002).

- [18] Y. Oh, A. I. Titov, and T.-S. H. Lee, Phys. Rev. C **63**, 025201 (2001).
- [19] D. Black, M. Harada, and J. Schechter, Phys. Rev. Lett **88**, 181603 (2002).
- [20] G. Erkol, G. E. Timmermans, and Th. A. Rijken, Phys. Rev. C **72**, 035209 (2005).
- [21] S. Ishida and K. Yamada, Phys. Rev. D **40**, 1497 (1988).
- [22] B.-G. Yu, T. K. Choi, W. Kim, Phys. Lett. B **701**, 332 (2011).
- [23] B.-G. Yu, K.-J. Kong, Phys. Lett. B **701**, 332 (2011).
- [24] N. I. Kochelev, D. P. Min, Y. Oh, V. Vento, and A. V. Vinnikov, Phys. Rev. D **61**, 094008 (2000).
- [25] D. V. Amelin et al., Z. Phys. C **66**, 71 (1995).
- [26] A. Liesenfeld et al., Phys. Lett. B **486**, 20 (1999).
- [27] A. Donnachie and Yu. S. Kalashnikova, Phys. Rev. C **93**, 025203 (2016).
- [28] M. Derrick et al. (ZEUS Collaboration), Z. Phys. C **73**, 73 (1996).
- [29] J. Ballam et al., Phys. Lett. B **30**, 321 (1969).
- [30] J. Busenitz et al., Phys. Rev. D **40**, 1 (1989).
- [31] M. Atkinson et al., Nucl. Phys. B **231**, 15 (1984).
- [32] D. Aston et al., Nucl. Phys. B **209**, 56 (1982).
- [33] R. M. Egloff et al., Phys. Rev. Lett. **43**, 1545 (1979).
- [34] W. Struczinski et al., Nucl. Phys. B **108**, 45 (1976).
- [35] Q. Zhao, Phys. Rev. C **63**, 025203 (2001).
- [36] H. Eberhardt et al., Phys. Lett. B **750**, 453 (2015).
- [37] Q. Zhao, Z. Li, and C. Bennhold, Phys. Rev. C **58**, 2393 (1998).
- [38] P. D. B. Collins and P. J. Kearney, Z. Phys. C **22**, 277 (1984).
- [39] M. N. Sergeenko, Z. Phys. C **64**, 315 (1994).
- [40] M. Williams et al. (CLAS Collaboration), Phys. Rev. C **80**, 065208 (2009).
- [41] M. Battaglieri et al. (CLAS Collaboration), Phys. Rev. Lett. **90**, 022002-1 (2003).
- [42] R. W. Clift et al., Phys. Lett. B **72**, 144 (1977).
- [43] M. Araki and A. N. Kamal, Phys. Rev. D **29**, 1345 (1984).
- [44] B.-G. Yu and K.-J. Kong, Phys. Lett. B **769**, 262 (2017).
- [45] G. Goldstein and J. F. Owens III, Nucl. Phys. B **71**, 461 (1974).
- [46] B.-G. Yu and K.-J. Kong, arXiv:1612.02071 [hep-ph].